Separation of NO$_x$ emissions from Drilling, and Oil and Gas Extraction in the U.S. using Monthly Data from the Ozone Monitoring Instrument

Master thesis by:

Joep de Bruin

in partial fulfillment of the requirements for the degree of

Master of Science

in Civil Engineering

at the Delft University of Technology

Geoscience & Remote Sensing department

Thesis committee:	Prof. dr. P.F. Levelt	TU Delft, KNMI
	Prof. dr. J.A. de Gouw	CU Boulder, CIRES
	Dr. T. Vlemmix	KNMI
	Dr. J.P. Veefkind	TU Delft, KNMI
	Dr. A. Barnhoorn	TU Delft

Table of Contents

Key points

- NO_x emissions can be explained by a linear combination of drilling and oil and gas extraction activities in the Permian, Bakken and Eagle Ford regions, but not elsewhere.
- Drilling and extraction are both important sources of NO_x emissions and together account for 50% of the total NO_x emissions in the Permian region.

Abstract

Horizontal drilling and hydraulic fracturing have increased unconventional oil and gas extraction from shale reserves in the U.S. in the last decade, making up more than half of total U.S. oil and gas production at present. This activity results in NO_x emissions in the extraction regions that are measurable from space using the Ozone Monitoring Instrument (OMI) on the NASA Aura satellite. The NO_x emissions are a result of two different activities: (1) the drilling and hydraulic fracturing of new wells, and (2) the extraction of oil and gas after the well is completed. To separate the NO_x emissions from drilling and extraction, a multiple linear regression to the NO_2 columns as a function of time is calculated for 9 extraction regions using the number of drilling rigs and the oil and gas extraction data from 2007 until 2018. In 3 regions (Permian, Bakken, Eagle Ford) a significant correlation between measured and modeled NO_2 columns is found, of which the Permian region shows the highest correlation. The analysis shows that half of the total NO_x emissions in the Permian region can be attributed to emissions from oil and gas activities, and that both the drilling and extraction activities have an equal share in the emissions. A fuel-based oil and gas emission inventory shows a different split for NO_x emissions from drilling and extraction in the Permian region, indicating drilling as the larger source. In other extraction regions, NO_2 columns show poor correlation with the oil and gas activities due to the proximity of urban areas (Barnett, Denver-Julesburg, Haynesville regions), power plants (San Juan) or variations in the drilling and extraction activity over time that are too small (Uintah, Upper Green River).

1. Introduction

1.1 Oil and Gas Production and Air Pollution

During the last decade, the production of oil and gas in the United States has increased by 100 and 50 percent, respectively (USEIA, 2018a, 2018b). These increases can be attributed to the advancements in the shale industry, in particular, the combination of two improved techniques: hydraulic fracturing and horizontal drilling. These techniques have made unconventional oil and gas resources economically viable and resulted in a surge of unconventional oil and gas production over the last decade. Today, unconventional oil and gas production makes up 50 and 75% of the total U.S. oil and gas production, respectively (EIA, 2018c). Unconventional oil and gas resources, also called tight oil and shale gas, are present in shale formations and can be found throughout the world (Howarth et al., 2011). However, only the U.S. has extracted these resources on a large scale in the past decade.

The increase of unconventional oil and gas production has resulted in an increase in emissions of several greenhouse gases and air pollutants (Howarth et al., 2011; Brandt et al., 2014). One of these pollutants is nitrogen oxide (NO_x), a family of trace gases consisting of nitric oxide (NO) and nitrogen dioxide (NO_2). NO_x is associated with direct health effects on the respiratory systems, even when health standards suggested by the WHO are met (WHO, 2005). Furthermore, NO_x plays a key role in the photochemical reactions that form ozone and fine particulate matter. Both ozone and fine particulate matter regularly exceed health standards in the U.S., Europe and other parts of the world, and are estimated to result in 2.5 million premature deaths globally per year (Silva et al., 2013). Ozone and fine particles also impact food security, causing more than 50% losses in wheat yield in strongly polluted regions (Burney & Ramanathan, 2014).

NO_x is efficiently produced during fossil fuel combustion where nitrogen and oxygen react. Within the oil and gas industry, NO_x emissions are associated with the use of heavy machinery and vehicles used to extract and transport the oil and gas, and other processes such as flaring (Kemball-Cook et al., 2010; Carlton et al., 2014; Ahmadov et al., 2015; Duncan et al, 2016). A distinction can be made between the drilling and extraction activity. During the drilling phase, heavy machinery is used to drill and hydraulically fracture the wells, and gases released during the process are combusted. During the extraction phase, NO_x emissions can come from dehydrators, heaters, separators, compressors, artificial lifts (i.e. pump jacks), transportation vehicles and in some cases flaring, when lighter hydrocarbons are combusted because the transportation and distribution of these gases is not economical (Gorchov Negron et al., 2018). Both drilling and extraction can have a significant effect on the NO_x concentration in the area. However, these processes operate on different time scales. The drilling and hydraulic fracturing of new wells takes weeks and this activity responds quickly to economic factors. The extraction of oil and gas from new wells continues for years and this activity responds only slowly to economic factors.

1.2 Prior Research: Satellite & In-situ Observations

Many studies have looked into NO_x emissions using in-situ or remote sensing instruments at the surface, on research aircraft, satellites or a combination of these methods. However, only few studies have specifically looked into the NO_x emissions from unconventional oil and gas production (Carlton et al., 2014) and the potential to form ozone (Schnell et al., 2009; Kemball-Cook et al., 2010; Edwards et al., 2014; McDuffie et al., 2016).

One previous study was done by Duncan et al. (2016) who used tropospheric NO_2 column measurements from the Ozone Monitoring Instrument (OMI) on board of NASA's Aura satellite to analyze changes in NO_x emissions above oil and gas extraction regions. These authors found that NO_2 columns increased by 10-30% between 2005 and 2014 above three of the major oil and gas extraction regions; the Bakken/Williston Basin in North Dakota, the Permian Basin in Texas & New Mexico, and the Eagle Ford area in Texas. The analysis also showed a "general match of shape between the area of NO_2 increases and distribution of nighttime lights in the regions, which suggests that the increases are associated with increased NO_x emissions from the oil and natural gas extraction activities" (Duncan et al, 2016).

Building on these findings, Majid et al. (2017) presented a quantitative trend analysis of NO_2 columns over seven U.S. shale regions (Bakken, Eagle Ford, Permian, Niobrara, Marcellus-Utica, Haynesville, and Barnett) between 2005 and 2015 using yearly averaged OMI measurements. These authors observed a rapid growth (1–4.5% yr^{-1}) in NO_2 columns over the most intensive oil-producing extraction regions (Bakken, Eagle Ford, Permian and Niobrara), which correlated well (r^2 = 0.6–0.9) with their annual oil production rates and drilling activity. In contrast, trends across the mainly gas-producing regions (Haynesville, Barnett, and Marcellus-Utica) show decreases (–0.4 to –1.7% yr^{-1}) similar to the national trend. Both Duncan's and Majid's analyses make use of NASA's version 3 OMI NO_2 standard product (Krotkov et al., 2017).

1.3 Introduction of this Work

The increased production of unconventional oil and gas between 2005 and 2014 resulted in higher NO_x emissions above several extraction regions. This is visible in the OMI data for three different extraction regions as shown by Duncan et al. (2016) and Majid et al. (2017). However, in the 2nd half of 2014, oil and gas prices dropped by 65 and 50%, respectively, resulting in regional decreases up to 80% in drilling activity and up to 30% in tight oil and shale gas extraction (USEIA, 2018d). These changes occurred on different time scales. While the decrease in drilling happened almost instantaneously (1 month) as result of the price drop, the extraction decreased on a longer timescale (1 year) due to the fact that production from a working well decreases only slowly in time. This difference in time scale may allow a quantitative separation of the effects of these activities on the total NO_x emissions.

This research continues with the tropospheric NO_x analysis above shale regions for two reasons; (1) to see whether the sharp downturn in drilling and extraction activity is visible in the NO_2 OMI data and (2) to quantitatively separate the effects of drilling and extraction on the total NO_x emissions. The analysis makes use of OMI measurements from 2005 to 2018 using KNMI's Dutch OMI NO_2 (DOMINO) product which is averaged per month (Boersma et al., 2011). Besides the Bakken, Permian and Eagle Ford basins, 6 other extraction regions will be investigated.

To support the outcomes of the OMI NO_2 columns, a comparison will be made with aerial in-situ measurements from the Shale Oil & Natural Gas Nexus (SONGNEX) campaign in 2015 (Koss et al., 2017; Peischl et al., 2018). During this campaign, measurements of multiple trace gases including NO_2 were performed using NOAA's WP-3D research aircraft. The measurements were made over 9 different shale regions including the Bakken, Permian and Eagle Ford basins. Furthermore, the results from the OMI analysis will be compared with the results from a fuel-based oil and gas emission inventory that estimates NO_x emissions from 7 different sources within the oil and gas production process (Gorchov Negron, 2018).

The following section will describe the used data sets; the NO_2 satellite observations from OMI, the NO_2 aircraft measurements made during the SONGNEX campaign and the oil and gas drilling and extraction data from the U.S. Energy Information Agency. Section 3, Results and Discussion, will explore the 9 different extraction regions and present a regression analysis that separates the NO_x emissions from drilling and from extraction. This section also includes two comparisons: (1) a comparison between the OMI NO_2 columns and the airborne NO_2 measurements from SONGNEX, and (2) a comparison between the drilling and extraction split calculated by the regression analysis and a split estimated from the emission inventory.

2. Data description

2.1 OMI NO_2 Column Observations

The Ozone Monitoring Instrument is a Dutch-Finnish instrument launched in 2004 on board of NASA's EOS-Aura satellite. The instrument contains a spectrometer that measures direct and backscattered sunlight in the UV-VIS window that ranges from 270-500 nm. The instrument has a spatial resolution of up to 13 km x 24 km at nadir and has a 2600 km viewing swath spanning 60 rows. The satellite moves in a sun-synchronous orbit, which passes the equator at approximately 13:30 local time and orbits the Earth 14 to 15 times a day, resulting in an almost global daily coverage. It measures several trace gases such as NO_2, SO_2, HCHO, O_3 and aerosols (Levelt et al., 2006, 2018).

The OMI NO_2 retrieval algorithm consists of three steps. First the NO_2 slant column densities (SCDs) are obtained from the OMI reflectance spectra using the Differential Optical Absorption Spectroscopy (DOAS) technique (Boersma et al., 2004). Then the SCDs are separated in a stratospheric and tropospheric part. The stratospheric contribution is estimated from assimilating slant columns into the chemical transport model TM4 (Boersma et al., 2007). Finally, the tropospheric SCDs are converted to vertical column densities (VCDs) using the tropospheric air mass factor (AMF) (Boersma, 2004, 2011). The end product is a tropospheric VCD (i.e. column), which signifies the total number of NO_2 molecules between the surface and the tropopause per cm^2.

The OMI NO_2 VCDs are part of the DOMINO v2.0 data product from the Royal Netherlands Meteorological Institute (KNMI) and are publicly available at www.temis.nl/airpollution/no2.html. This is a Level 2 product, meaning it contains geophysical variables at the same resolution and location of the satellite's ground pixel. This is different from NASA's Level 3 product used by Duncan et al. (2016) and Majid et al. (2017) which is binned and averaged on a uniform grid.

Since June 2007 several anomalies occurred in the instrument's 60 individual viewing angles (rows) (Schenkeveld et al., 2017). These row anomalies resulted in unreliable data in the rows 25-55 and are excluded from the dataset in order to obtain a reliable trend analysis. The rows 1-4 and 56-60 are also excluded from the dataset due to their large ground pixel size, resulting in a dataset that uses the rows 5-25. Furthermore, individual pixels with cloud fractions above 0.2 and surface albedos above 0.3 are removed from the dataset to minimize the retrieval uncertainties from clouds and aerosols (Boersma et al., 2011). In 2016 and 2017 some measurement days are missing due to problems with the satellite. However, this does not result in any gaps in the dataset because the data is averaged per month.

The OMI NO_2 VCDs are used in this work as a proxy for NO_x emissions, which makes three assumptions. First, NO_x is dominated by NO_2, especially when averaged over larger areas. Second, when studying

trends in NO_2 VCDs it is assumed that the NO/NO_2 ratio is not changing in time. Third, because of the short lived tropospheric lifetime of NO_x (3-5 hours), it can be assumed that regional enhancements in NO_2 columns are caused by emissions in that same region (Lin et al., 2010). The link between OMI NO_2 columns and NO_x emissions is visible on monthly and yearly timescales (Duncan et al., 2013) and OMI NO_2 columns have been used as a proxy for NO_x emissions in several oil and gas extraction regions in the U.S. and Canada (Duncan et al., 2016; Li et al., 2016; Majid et al., 2017).

2.2 SONGNEX NO_2 Observations

The Shale Oil & Natural Gas Nexus was an airborne measurement campaign that measured trace gases and fine particles above several tight oil and shale gas basins in the western United States. The goal was to understand the atmospheric effects of the changing energy use in the U.S. by quantifying the emissions of trace gases and fine particles above extraction regions and study the chemical transformation of these emissions (Koss et al., 2017; Peischl et al., 2018).

The measurements were performed in March and April 2015 in 9 extraction regions, which represent a mix of tight oil and shale gas production regions at different stages of development; the Bakken, Permian, Eagle Ford, Haynesville, Barnett, San Juan, Denver-Julesburg, Uintah and the Upper Green River basin (Figure 1). The measurements were done using a wide set of instruments on board of the WP-3D research aircraft from the National Oceanic and Atmospheric Administration (NOAA). More details on the mission can be found at www.esrl.noaa.gov/csd/projects/songnex/.

In this paper we make use of NO_2 measurements by chemiluminescence detection and of various position and meteorological parameters such as altitude, temperature and pressure (Warneke et al., 2016). A total of 19 measurement flights were performed, meaning most extraction regions were studied on multiple days. Each measurement day provided a horizontal measurement distribution of the entire extraction region and several spirals up to 3 km above ground level probed the depth of the boundary layer. Some flights have a higher vertical range of up to 7 km.

2.3 Oil & Gas Extraction and Drilling Data

The U.S. Energy Information Administration (USEIA) provides data on the oil and gas production in 7 key extraction regions (Bakken, Eagle Ford, Permian, Niobrara, Appalachia/Marcellus, Haynesville, and Anadarko). The data starts in January 2007, is aggregated per month and consists of three parts; oil extraction, gas extraction and the number of active drilling rigs (i.e. rig count).

The oil and gas extraction are quantified in barrels/day and ft^3/day, respectively, and are reported by industry to the individual states. The extraction data is not limited to tight or shale formations, meaning part of the extraction data comes from conventional sources. The data signifies the extraction of oil and gas for both new and existing wells in the region. Where state data is not available, the USEIA estimates the extraction based on the number of wells (USEIA, 2018d).

The rig count is a census of the number of drilling rigs actively exploring for or developing oil or natural gas (Baker Hughes, 2018). The USEIA obtains the rig count data from Baker Hughes, a data company which maintains frequent contact with the drilling operators. The USEIA does not distinguish between oil-directed and gas-directed rigs because once a well is completed it can produce both oil and gas (USEIA, 2018d). Additional production data from other regions (Barnett, San Juan, Denver-Julesburg, Uintah and the Upper Green River basin) come from state databases which where aggregated by Koss et al. (2017).

3. Results and Discussion

3.1 OMI NO$_2$ Columns in 9 major Extraction Regions

Figure 1 shows the absolute changes in tropospheric NO$_2$ VCDs from OMI between 2005 and 2014 on a grid with a resolution of 0.5° by 0.5°. It shows NO$_2$ decreases in the eastern part of the U.S. and in several urban regions in the west, corresponding with NO$_x$ emission decreases in cities due to stricter regulations (Russel et al., 2012; McDonald et al., 2012). Other regions in the western part show little change or increases in NO$_2$ columns.

The figure also shows the outlines of 9 major extraction regions in the United States. The outlines of these extraction regions are based on the location of oil and gas wells, drilling rigs and other anthropogenic NO$_2$ sources. In this paper, we will study the average NO$_2$ columns over these regions. Three of these regions are also studied by Duncan and Majid (Bakken, Permian, Eagle Ford), two more are studied only by Majid (Haynesville, Barnett) and four are not studied in these previous articles (San Juan, Denver-Julesburg, Uintah, Upper Green River).

The Eagle Ford, Barnett and Denver-Julesburg regions are located close to large cities (San Antonio, Dallas and Denver, respectively) that saw decreases of NO$_x$ emissions in the last decade and can influence the NO$_2$ columns above the extraction regions (Russel et al., 2012). The Haynesville region does not border a large city but does have a high concentration of smaller cities and is further East, where NO$_2$ columns are trending down everywhere. In the San Juan region several power plants are present (e.g. Four Corners) that saw decreases in their NO$_x$ emissions in recent years due to emission control systems (Kim et al., 2006). The Bakken, Permian, Uintah and Upper Green River extraction regions are located far away from other anthropogenic sources of NO$_x$ such as large cities or power plants, making them the most suited for this analysis. Not included in this analysis is the Marcellus region in Pennsylvania, which is strongly affected by NO$_x$ emissions from nearby and large urban areas.
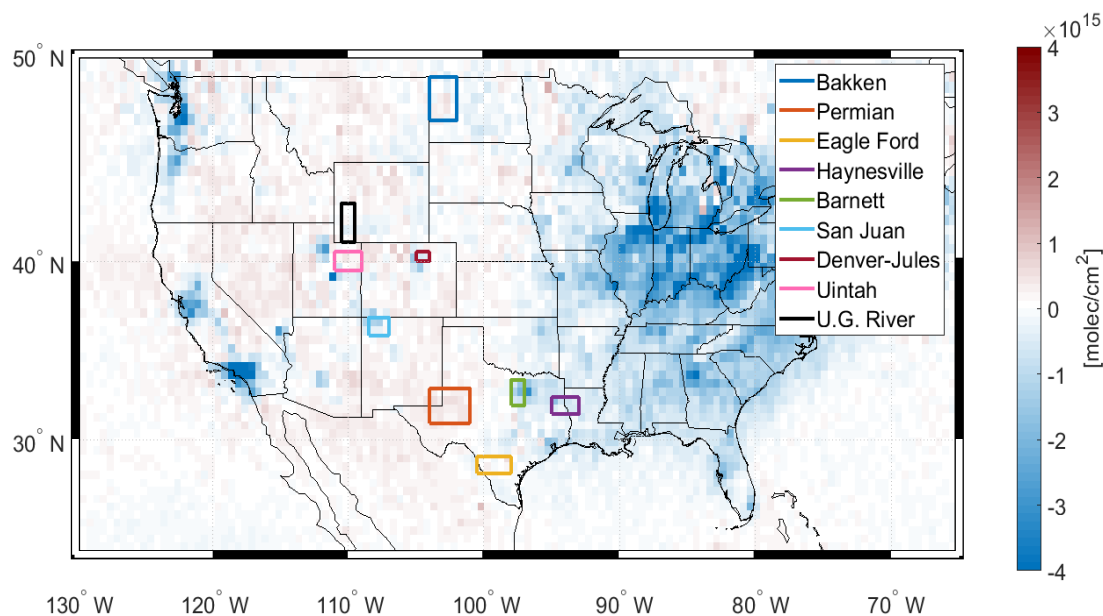
Figure 1. The absolute changes (x10^{15} molecules/cm^2) in OMI NO$_2$ column data between 2005 and 2014 for the continental U.S. (0.5° latitude x 0.5° longitude). For clarity, the color bar is clipped to -4 and +4 x10^{15} molecules/cm^2 but in some urban areas actual changes are larger. The colored outlines represent the 9 extraction regions which are investigated in this research.

Figure 2 shows the tropospheric NO$_2$ column, rig count, oil extraction and gas extraction in the 9 extraction regions for three important years; 2007, 2014 and 2016. In 2007, when oil and gas production was lower in most of these regions, the USEIA started to track the drilling and extraction activity per region. In 2014, when the oil price was still high, the drilling and extraction of tight oil peaked in most regions. In 2016, drilling had decreased dramatically in these regions as a result of the price drop in 2014 and 2015, while extraction showed smaller decreases (Eagle Ford, Bakken) or even small increases (Permian). Drilling and extraction increased again in 2017 as result of oil price increases.

The figure shows that most of the oil extraction happens in the Bakken, Permian and Eagle Ford regions, while gas extraction is distributed over all regions. These 3 oil-producing regions, which also showed up in Duncan's study, saw large increases in drilling and extraction activity between 2007 and 2014, as well as an increase in NO$_2$ columns in the same period. Between 2014 and 2016 these regions saw dramatic decreases in drilling activity while extraction stayed more constant. While a downturn in the NO$_2$ columns is visible for the Bakken and Permian region between 2014 and 2016, the NO$_2$ columns did not decrease as strongly as the drilling activity, indicating that drilling is not the only dominant source of NO$_x$ emissions in these regions.

The Haynesville, Barnett, San Juan and Denver-Julesburg regions show much higher NO$_2$ columns due to the proximity of other NO$_x$ sources such as cities and power plants. The NO$_2$ columns in these regions mostly decreased, which can be attributed to a reduction in NO$_x$ emissions from other combustion sources. The Uintah and Upper Green River basins show the smallest variations in NO$_2$ columns due to little change in extraction and the absence of other, large NO$_x$ sources in the area.
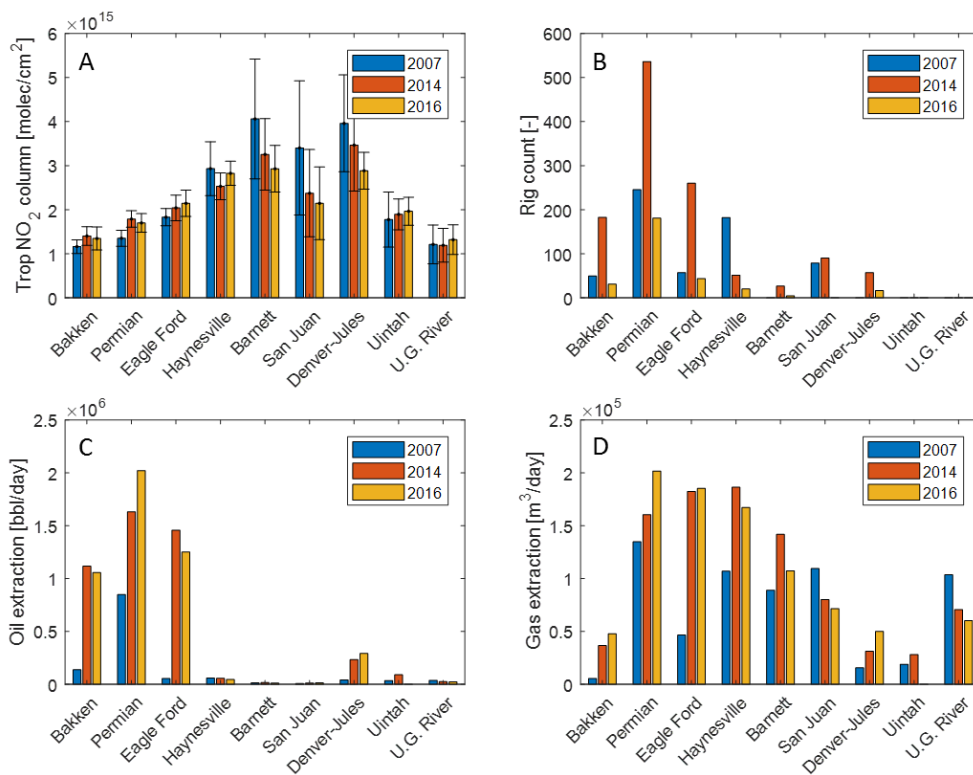
Figure 2. (A) The tropospheric OMI NO$_2$ columns, (B) number of drilling rigs, (C) extraction of oil and (D) extraction of gas in the years 2007, 2014 and 2016 for the 9 extraction regions. The error bars in the (A) depict the standard deviation. Rig count data is missing for the Uintah and Upper Green River basins, as well as in the Barnett and Denver-Julesburg regions for 2007.

The tropospheric NO_2 columns in the extraction regions have seasonal cycles that originate from variations in sun hours and solar angle, which influence the lifetime of NO_2 (Boersma et al., 2009). In summer, with more sunlight, NO_2 is transformed more efficiently into NO_y with ozone as a by-product, resulting in lower NO_2 columns and higher ozone columns, while in winter the opposite is true.

The seasonal variation in NO_2 columns is present in all extraction regions, but the amplitude of the seasonal variation changes per region. To account for this, the seasonal cycle is normalized using the normalized seasonal cycles shown in Figure 3. These curves were calculated by dividing the average monthly columns by the average annual column. Both monthly and annual columns are averaged of the 13 years of OMI data. These normalized, average seasonal variations will be used in Section 3.2 to remove the seasonal effect from the monthly time series. Our method to remove the seasonal variation in the OMI time series is somewhat different from other studies that used fits of sinusoidal functions to the data (Van der A et al, 2008). We adopted a different approach here, because (1) the seasonal variation is not exactly sinusoidal, and (2) the trends over time we are interested in can also affect the amplitude of the seasonal cycle.

Since the seasonal cycle is dominated by the variability in sun hours and solar angle, we predict a stronger seasonal variation in the northern extraction regions. This is consistent with the cycles in Figure 3 for all regions except the Bakken region, which shows a relative weak seasonal cycle for its latitude. This can be caused by missing data points in this region during the winter months, due to more clouds and snow that interfere with the OMI retrievals.
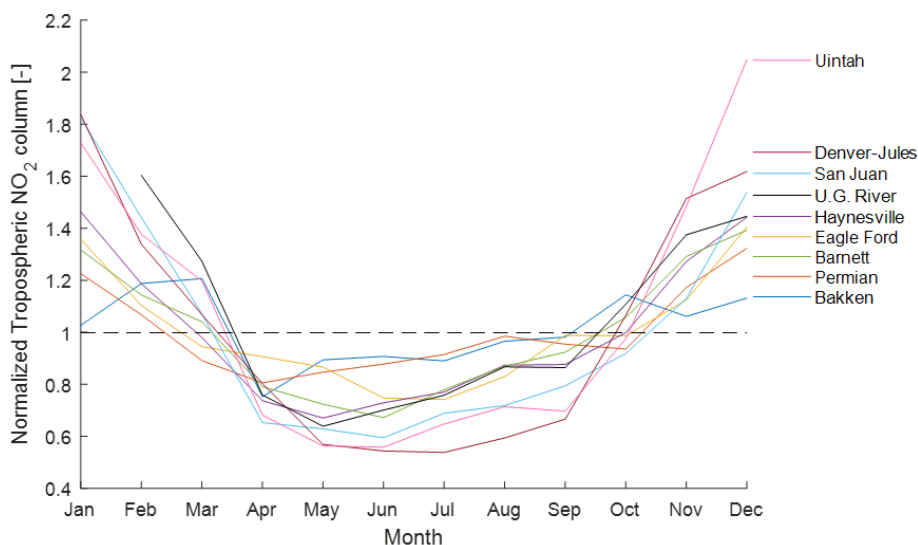
Figure 3. The normalized tropospheric NO_2 columns averaged per month for 13 years (2005-2018) and divided by its mean value for the 9 extraction regions.

3.2 Regression Analysis of NO_2 Trends

The monthly averaged time series of the tropospheric NO_2 column from 2005 till 2018 in the Permian region is shown in Figure 4. The seasonal variation of the NO_2 column is removed from the time series using the normalized seasonal cycles shown in Figure 3 (see S.I.). The seasonal variation is not caused by the emissions from oil and gas and can therefore be removed in order to better compare the NO_2 column with the drilling and extraction data.

Besides the NO_2 column, Figure 4 also shows the number of active drilling rigs and the extraction of oil in the Permian region from 2007 till 2018. The rig count and oil extraction have different time series, while oil extraction and gas extraction have very similar time series because oil and gas are often extracted from the same wells in this region (see S.I.). A comparison of the NO_2 column with the production data shows that neither the rapidly changing number of drilling rigs, nor the more constant extraction data can fully account for the changes in the NO_2 column. This also shows up in a regression between the NO_2 column and the drilling and oil extraction data (r^2 = 0.196 and 0.298, respectively) which is presented in Table 1. Combining the drilling rig and extraction data could improve the NO_2 column estimation.
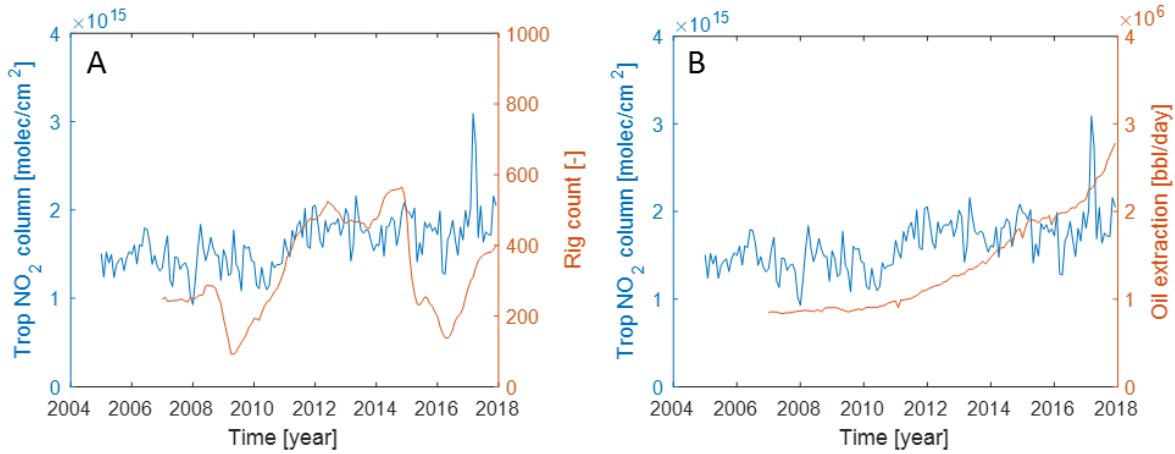
Figure 4. The tropospheric NO_2 column time series, averaged per month, from 2005 to 2018 (blue) plotted with (A) the number of drilling rigs and (B) the extraction of oil from 2007 to 2018 (orange). The seasonal variation is removed from the NO_2 time series.

The effects of drilling and extraction can be combined using a multiple linear regression to the NO_2 column as a function of time, as described by:

$$NO_2(t) = B + F_{rig} \times A_{rig}(t) + F_{ext} \times A_{ext}(t)$$

The constant B describes the NO_2 background column in the area, signifying the NO_2 column from natural sources and anthropogenic sources not related to oil and gas production. The other components (rig count & extraction) describe the effect of their respective activity on the total NO_x emissions in the area and both consist of two parts; the original drilling rig or extraction activity data (A_{rig} and A_{ext}) that changes in time, and an emission factor (F_{rig} and F_{ext}) that is constant in time. The emission factors, calculated from the regression, translate the activity into NO_2 columns and describe the sensitivity of the NO_x emissions to that activity. The regression also calculates a coefficient of determination (r^2) that describes the correlation between the modeled and the measured NO_2 columns in time. This regression is done for all extraction regions using the number of drilling rigs and the oil and gas extraction data from 2007 till 2018. The background column, emissions factors and coefficients of determination (r^2) for the Permian region are presented in Table 1 for seven different combinations. The table shows that a multiple linear regression with the combination rig + oil results in the strongest correlation (r^2 = 0.433), meaning that a combination of drilling activity and oil extraction explains 43% of the variability in the measured NO_2 time series in this region. This combination of drilling and oil extraction fits the NO_2 column better then one of these activities separately (r^2 = 0.196 and 0.298), showing that both activities are important sources of NO_x emissions.

The combination rig + oil correlates stronger with the NO_2 time series than a combination of rig + gas (r^2 = 0.407). Similarly, the individual oil extraction correlates better with the NO_2 column than the individual gas extraction (r^2 = 0.298 vs 0.171), meaning oil extraction describes the NO_2 time series better. For this reason, the analysis focuses on the extraction of oil as the more important driver of NO_x emissions from extraction.

The table also shows that a combination of oil + gas results in a negative emission factor, meaning the regression results are not physically meaningful for this combination. This happens because the oil extraction and gas extraction have similar time series, which makes it difficult for the regression to distinguish between them. When using a combination of drilling, oil extraction and gas extraction, the 95% confidence intervals become larger than the calculated emissions factors, meaning the results are insignificant. For all other combinations the emission factors are significant, which shows that this regression analysis can be used to quantify the contributions from drilling and extraction to the total NO_x emissions.

Table 1. Results from the multiple linear regression including; the background column, emission factors for rig count, oil extraction and gas extraction and the coefficient of determination (r^2) for 7 different input combinations in the Permian region.

Permian region	Background ($\times 10^{15}$) [molec/cm^2]	Rig Factor ($\times 10^{11}$) [molec/cm^2/rig]	Oil Factor ($\times 10^{8}$) [molec/cm^2/bbl/day]	Gas Factor ($\times 10^{9}$) [molec/cm^2/m^3/day]	r^2
Rig	1.31 ±0.13	10.30 ±3.64	-	-	0.196
Oil	1.21 ±0.12	-	3.19 ±0.85	-	0.298
Gas	1.12 ±0.28	-	-	3.44 ±1.31	0.171
Rig + Oil	0.97 ±0.14	8.68 ±3.09	2.88 ±0.77	-	0.433
Rig + Gas	0.68 ±0.21	11.41 ±3.15	-	3.86 ±1.31	0.407
Oil + Gas	1.56 ±0.27	-	7.57 ±2.46	-6.29 ±3.54	0.370
All	0.85 ±0.48	8.36 ±4.74	2.78 ±3.58	0.74 ±5.3	0.437

Figure 5 shows the tropospheric NO_2 time series measured by OMI, and the modeled NO_2 time series with the strongest correlation, the rig + oil combination, in the Permian region. The modeled NO_2 time series is split by its three components (background, rig count & oil extraction) to see the contributions of each component to the total NO_2 column. When quantifying the emission sources, the figure shows that drilling and extraction both contribute to the NO_2 column but the relative importance varies in time as the intensity of the drilling and extraction activities change. The figure also shows that the emissions from drilling and extraction combined, can be as large as all the other natural and anthropogenic sources of NO_2 (i.e. the background), meaning that the production of oil effectively doubles the NO_2 column in the area.

The regression coefficients improve when the seasonal variation of the NO_2 column is removed using a 12-month running mean instead of the normalized seasonal cycles (r^2 ~ 0.8, see S.I.). And when NO_2 column data, drilling and extraction data are averaged per year instead of per month the correlation between the measured and modeled NO_2 time series also improves (r^2 ~ 0.8, see S.I.). In both cases the correlations are higher compared to the original monthly time series that use the normalized seasonal cycles from Figure 3, which is expected since the new NO_2 time series are smoother. However, we present the monthly data in Figure 5 because the abrupt changes in drilling occurred on such timescales and we are interested in the corresponding changes in NO_2 columns.
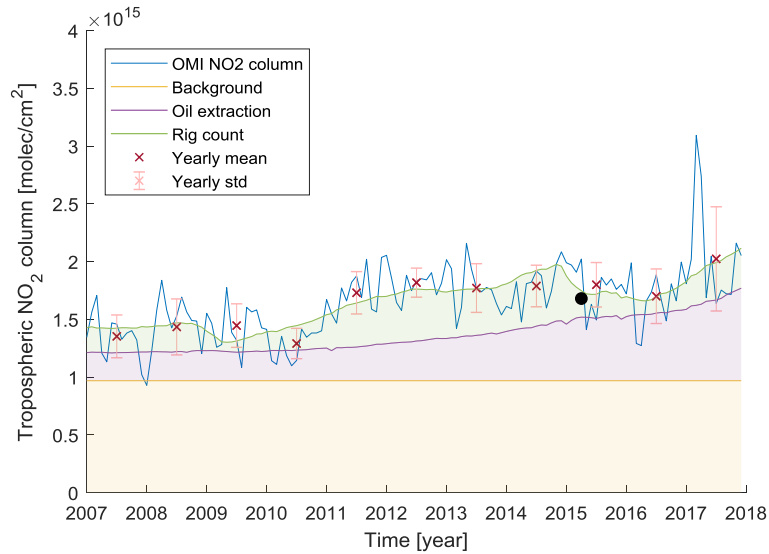
Figure 5. The measured tropospheric OMI NO$_2$ column time series (blue) and the modeled NO$_2$ time series separated in a constant background column (yellow), an NO$_2$ column caused by extraction of oil (purple) and an NO$_2$ column caused by drilling (green) in the Permian region. The red crosses and error bars represent the yearly averages and standard deviations of the measured NO$_2$ time series. The black dot represents the SONGNEX column described in Section 3.3.

The multiple linear regression is repeated for different region sizes in order to check the sensitivity of the analysis. The different areas are depicted in Figure 6a and the corresponding regression results are shown in Figure 6b-e. The figure shows that when the size of the region increases; (1) the correlation between the modeled and measured NO$_2$ column weakens (6b), (2) the emission factors for drilling and extraction decrease (6d-e) and (3) the background signal stays constant (6c). These three outcomes show that drilling and oil extraction are the dominant driving factor for the trends in the NO$_2$ column over the Permian region, but not outside of it. The results are particularly convincing when considering that the larger regions (region 2 and 3) also show an increasing NO$_2$ trend (Figure 6a) but that these increases do not correlate with the drilling and extraction time series.
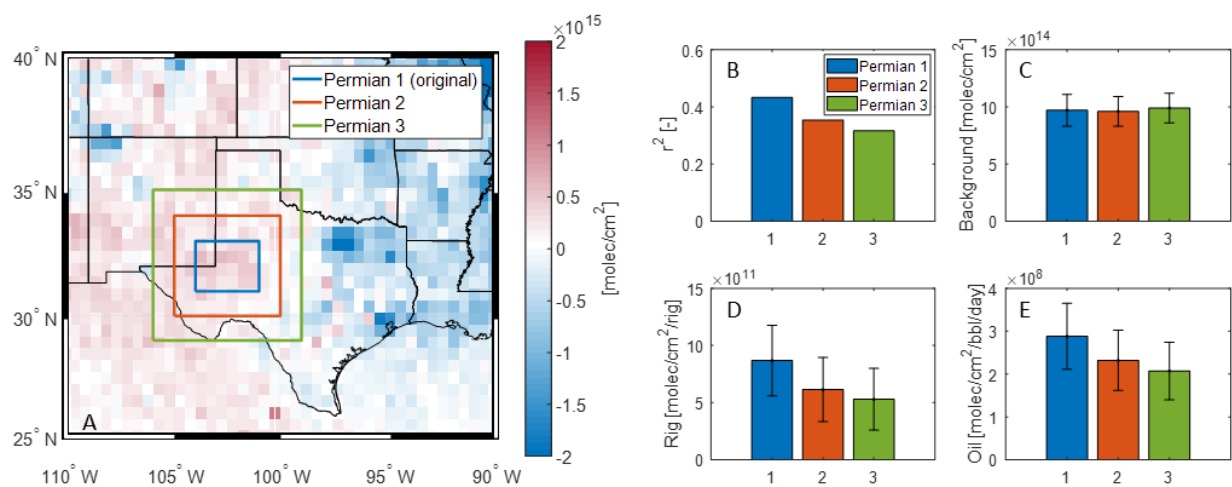
Figure 6. (A) The absolute changes in OMI NO$_2$ column data between 2005 and 2014 and the outlines of the original Permian region used for the regression analysis (blue) and two larger regions (orange & green). (B) The coefficient of determination, (C) the background column, (D) the emission factor for drilling and (E) the emission factor for oil extraction for the three Permian region sizes.

13

The analysis is repeated for all extraction regions in Figure 1 (see S.I.). The NO_2 time series of the Permian, Bakken and Eagle Ford regions show a correlation with the drilling and extraction data and the resulting correlation coefficients, background columns and emissions factors are presented in Figure 7. In the other 6 extraction regions, the NO_2 time series show no correlation with the drilling or extraction data, which can be explained by the proximity of urban areas (Barnett, Denver-Julesburg, Haynesville), power plants (San Juan) or variations in the drilling and extraction activity over time that are relatively small (Uintah, Upper Green River).

Both the Bakken and the Eagle Ford regions show weaker correlations (r^2 = 0.15 and 0.12, respectively) than the Permian region for a combination of rig count and oil extraction (Figure 7a). In the Bakken region, the correlation is limited by missing data points in the NO_2 time series during some winters, due to the higher latitude of the region with more clouds and snow that interfere with the OMI retrievals. In the Eagle Ford region, the weaker correlation may be caused by the NO_x emissions from the city of San Antonio, which is near the extraction region. The emissions from the city may also explain the higher background column in this region compared to the Permian and Bakken regions (Figure 7b). The emission factors for the oil extraction are significant in all three regions and the emission factors for rig count are significant in the Permian and Eagle Ford regions. The figure shows that the emission factors vary per region but are within each other's uncertainties (Figure 7c-d). The regional variation can be caused by the use of different machinery, a different composition of the oil and gas resources or by differences in the meteorology.

Combining the emission factors from the three regions gives averaged emission factors of F_{rig}= 6.6 x 10^{11} molecules/cm^2/rig and $F_{ext,oil}$= 2.6 x 10^8 molecules/cm^2/barrel/day. These factors can be used to estimate the emissions from drilling and extraction on the total NO_2 column in more complex extraction regions where no direct correlation is found. In the Denver-Julesburg region, this estimation shows that drilling and oil extraction account for a maximum of 0.11 x 10^{15} molecules/cm^2 (in December 2014), which is only 3% of the total NO_2 column in the region. This small percentage likely explains why no correlation was found between the NO_2 time series and the drilling and extraction data in the Denver-Julesburg region.
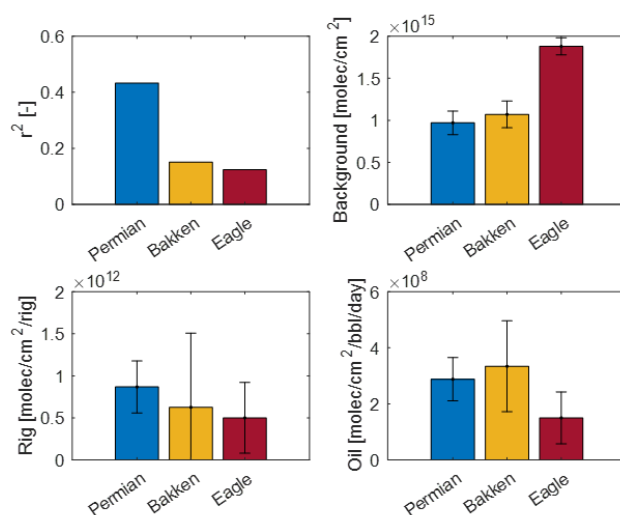
Figure 7. (A) The coefficient of determination, (B) the background column, (C) the emission factor for drilling and (D) the emission factor for oil extraction for the Permian, Bakken and Eagle Ford extraction regions.

3.3 SONGNEX NO$_2$ Profile and Column Comparison

During the SONGNEX campaign, airborne in-situ NO$_2$ measurements were made in the 9 extraction regions presented in Figure 1. The measurements are used to calculate vertical NO$_2$ profiles. The NO$_2$ profile for the flight over the Permian region is presented in Figure 8. The profile shows that most of the NO$_2$ molecules are situated in the lowest 2 km of the troposphere (i.e. the boundary layer). This is consistent with our finding that the column NO$_2$ measurements are correlated with surface emissions of NO$_x$. Above 2 km altitude, in the free troposphere, the profile shows a more constant NO$_2$ concentration which is not related to the NO$_x$ emissions on the surface.

In order to compare the NO$_2$ profile with the OMI NO$_2$ column, the profile is extrapolated to the tropopause (10 km for the Permian) and converted into a column by integrating the NO$_2$ concentration over the height. The NO$_2$ column calculated from the aircraft data (1.7 x 10^{15} molecules/cm^2) is added in Figure 5 (black dot) and is in the range of NO$_2$ columns observed from OMI. Integrating the free tropospheric average (yellow line in Figure 8) over the entire troposphere including the boundary layer gives an NO$_2$ column of 0.7 x 10^{15} molecules/cm^2, which can be interpreted as the background column in the absence of surface emissions in the region. This value is somewhat smaller than the background column derived from the multiple linear regression in Figure 5, which is (0.97$\pm$0.14) x 10^{15} molecules/cm^2 (Table 1). This is consistent with our finding that most of the enhancement in the NO$_2$ column can be attributed to enhanced NO$_2$ concentrations in the boundary layer due to oil and gas production. The small difference between the two background columns can be attributed to the assumption that the free tropospheric profile is constant with height, while in reality the profile will increase towards the surface as the pressure increases.
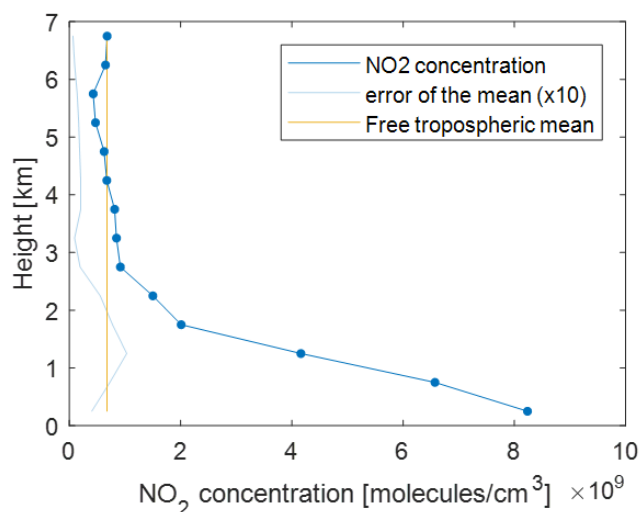
Figure 8. NO$_2$ profile in the Permian region between the surface and 7 km altitude, averaged in bins of 500 meter (blue) and its error of the mean which is multiplied by 10 for clarity purposes (light blue). The yellow line describes the average concentration between 2.5 and 7 km.

3.4 Comparison with a Fuel-Based Oil and Gas Inventory

In Section 3.2 we distinguished between the NO_x emissions from drilling and extraction using a multiple linear regression of OMI NO_2 column data. Another approach is to estimate NO_x emissions directly from the NO_x producing activities using an emission inventory and emission factors. This is done by Gorchov Negron et al. (2018) who developed a fuel-based oil and gas inventory to estimate NO_x emissions from different sources in the oil and gas production process. The inventory contains 7 different NO_x emission sources for several extraction regions, including the Permian region, for which the emissions are presented in Table 2.

According to the inventory, 88% of total NO_x emissions from the oil and gas production in the Permian basin are associated with drilling, while the other 6 sources representing the extraction activity make up only 12%. This is different from the split found in our work, which shows a 52 versus 48% ratio for drilling versus extraction in 2013 (the year the inventory data is based on), with an estimated uncertainty of $\pm11\%$. The difference may be due to uncertainties in the drilling emission factor used in the inventory. This drilling emission factor is 1.9 g NO_x/cm drilled, with an uncertainty of +4.7/-1.5 g NO_x/cm. As a result, the NO_x emission from drilling has an uncertainty of +366/-119 metric tons NO_x/day. This translates into an uncertainty in the split between drilling and extraction in the inventory of +8/-26%. However, the uncertainties in the split from the analysis of OMI data and from the inventory do not fully account for the difference in the splits. It should also be noted that the inventory covers only the part of the Permian basin in Texas, whereas the satellite data was averaged over the production in Texas and New Mexico (Figure 1).

Furthermore, the table shows that 6.6% of NO_x emissions come from artificial lifts, which are associated with oil extraction. The dehydrators, heaters, compressors and processing plants, which represent the gas extraction, produce 5.2% of the total NO_x emission. Although the difference is not large, this makes oil extraction the larger source of the two, which is in line with the results from the multiple linear regression presented in Table 1 in Section 3.2.

Table 2. Emission estimates from the fuel-based oil and gas inventory for the Permian region (Gorchov Negron et al., 2018).

NO_x source	Emission [metric tons NO_x/day]	Emission share [%]
Dehydrator	0.08	0.0
Heater	0.26	0.2
Lateral Compressors	0.79	0.5
Wellhead Compressors	3.22	1.9
Processing Plant	4.71	2.7
Artificial Lifts	11.43	6.6
Drilling	153.36 (+366/-119)	88 (+8/-26)
Total	173.85	100.0

4. Conclusions

In this paper we show that a multiple linear regression of oil and gas production data to the OMI NO_2 column time series can separate and quantify the contributions from drilling and extraction on the total NO_2 column in the Permian, Bakken and Eagle Ford extraction regions. The regression analysis shows that drilling and extraction are both important sources of NO_x emissions and together account for 50% of the total NO_2 column in the Permian region. The Bakken and Eagle Ford regions show weaker correlations than the Permian but show significant effects from drilling and extraction on the total NO_2 column. In other extraction regions, NO_2 time series show no correlation with the drilling or extraction data, which can be explained by the proximity of urban areas (Barnett, Denver-Julesburg, Haynesville), power plants (San Juan) or variations in the drilling and extraction activity over time that are too small (Uintah, Upper Green River).

A comparison with a fuel-based oil and gas emission inventory shows that the split between the effects of drilling and extraction on the total NO_2 column derived from the multiple linear regression and from the emission inventory are different. The regression analysis attributes 52 $\pm$11% to drilling, while the inventory attributes 88% (range 62%-96%) to drilling, with the remainder in each case from extraction.

In the future, these types of analyses can be done in much more detail using the improved spatial resolution (7 km x 3.5 km) and sensitivity obtained with the recently launched Tropospheric Monitoring Instrument (TROPOMI).

Acknowledgments and Data

References

Baker Hughes (2018). 6 March. [Available at: http://phx.corporate-ir.net/phoenix.zhtml?c=79687&p=irol-rigcountsfaqs]

Boersma, K. F., Eskes, H. J., & Brinksma, E. J. (2004). Error analysis for tropospheric NO2 retrieval from space. *Journal of Geophysical Research: Atmospheres*, *109*(D4).

Boersma, K. F., Eskes, H. J., Veefkind, J. P., Brinksma, E. J., Van Der A, R. J., Sneep, M., ... & Bucsela, E. J. (2007). Near-real time retrieval of tropospheric NO 2 from OMI. Atmospheric Chemistry and Physics, 7(8), 2103-2118.

Boersma, K. F., Jacob, D. J., Trainic, M., Rudich, Y., DeSmedt, I., Dirksen, R., & Eskes, H. J. (2009). Validation of urban NO 2 concentrations and their diurnal and seasonal variations observed from the SCIAMACHY and OMI sensors using in situ surface measurements in Israeli cities. *Atmospheric Chemistry and Physics*, *9*(12), 3867-3879.

Boersma, K. F., Eskes, H. J., Dirksen, R. J., Veefkind, J. P., Stammes, P., Huijnen, V., ... & Richter, A. (2011). An improved tropospheric NO2 column retrieval algorithm for the Ozone Monitoring Instrument. Atmospheric Measurement Techniques, 4(9), 1905.

Brandt, A. R., Heath, G. A., Kort, E. A., O'Sullivan, F., Petron, G., Jordaan, S. M., Tans, P., Wilcox, J., Gopstein, A. M., Arent, D., Wofsy, S., Brown, N. J., Bradley, R., Stucky, G. D., Eardley, D. and Harriss, R. (2014). Methane Leaks from North American Natural Gas Systems, Science, 343(6172), 733–735, doi:10.1126/science.1247045.

Burney, J., & Ramanathan, V. (2014). Recent climate and air pollution impacts on Indian agriculture. Proceedings of the National Academy of Sciences, 111(46), 16319-16324.

Carlton, A. G., Little, E., Moeller, M., Odoyo, S., & Shepson, P. B. (2014). The data gap: can a lack of monitors obscure loss of clean air act benefits in fracking areas? Environ. Sci. Technol., 48, 893, 2014.

Dirksen, R. J., Boersma, K. F., Eskes, H. J., Ionov, D. V., Bucsela, E. J., Levelt, P. F., & Kelder, H. M. (2011). Evaluation of stratospheric NO2 retrieved from the Ozone Monitoring Instrument: Intercomparison, diurnal cycle, and trending. Journal of Geophysical Research: Atmospheres, 116(D8).

Duncan, B. N., Lamsal, L. N., Thompson, A. M., Yoshida, Y., Lu, Z., Streets, D. G., ... & Pickering, K. E. (2016). A space-based, high-resolution view of notable changes in urban NOx pollution around the world (2005–2014). Journal of Geophysical Research: Atmospheres, 121(2), 976-996.

Duncan, B. N., Yoshida, Y., de Foy, B., Lamsal, L. N., Streets, D. G., Lu, Z., ... & Krotkov, N. A. (2013). The observed response of Ozone Monitoring Instrument (OMI) NO2 columns to NOx emission controls on power plants in the United States: 2005–2011. Atmospheric environment, 81, 102-111.

Edwards, P. M., Brown, S. S., Roberts, J. M., Ahmadov, R., Banta, R. M., de Gouw, J. A., Dube, W. P., Field, R. A., Flynn, J., Gilman, J. B., Graus, M., Helmig, D., Koss, A. R., Langford, A. O., Lefer, B. L., Lerner, B. M., Li, R., Li, S. M., McKeen, S. A., Murphy, S. M., Parrish, D. D., Senff, C. J., Soltis, J., Stutz, J., Sweeney, C., Thompson, C., Trainer, M. K., Tsai, C., Veres, P. R., Washenfelder, R. A., Warneke, C., Wild, R. J., Young, C. J., Yuan, B. and Zamora, R. (2014). High winter ozone pollution from carbonyl photolysis in an oil and gas basin, Nature, 514, 351–354.

Gorchov Negron, A., McDonald, B.C., McKeen, S.A., Peischl, J., Ahmadov, R., de Gouw, J.A., Frost, G.J., Hastings, M., Ryerson, T.B., Thompson, C., Trainer M. (2018, in review). Development of a Fuel-Based Oil and Gas Inventory of Nitrogen Oxide Emissions. Environment Science and Technology.

Howarth, R. W., Ingraffea, A., & Engelder, T. (2011). Natural gas: Should fracking stop?. *Nature*, *477*(7364), 271.

Kemball-Cook, S., Bar-Ilan, A., Grant, J., Parker, L., Jung, J., Santamaria, W., Mathews, J. and Yarwood, G. (2010). Ozone impacts of natural gas development in the Haynesville shale, Environ. Sci. Technol., 44, 9357–9363.

Kim, S. W., Heckel, A., McKeen, S. A., Frost, G. J., Hsie, E. Y., Trainer, M. K., ... & Grell, G. A. (2006). Satellite-observed US power plant NOx emission reductions and their impact on air quality. *Geophysical Research Letters*, *33*(22).

Koss, A., Yuan, B., Warneke, C., Gilman, J. B., Lerner, B. M., Veres, P. R., Peischl, J., Eilerman, S., Wild, R., Brown, S. S., Thompson, C. R., Ryerson, T., Hanisco, T., Wolfe, G. M., St Clair, J. M., Thayer, M., Keutsch, F. N., Murphy, S. and de Gouw, J. A. (2017). Observations of VOC emissions and photochemical products over US oil- and gas-producing regions using high-resolution H3O+ CIMS (PTR-ToF-MS), Atmos. Meas. Tech., 10, 2941–2968, doi:10.5194/amt-2017-103.

Krotkov, N. A., Lamsal, L. N., Celarier, E. A., Swartz, W. H., Marchenko, S. V., Bucsela, E. J., Chan, K. L., Wenig, M., & Zara, M. (2017). The version 3 OMI NO 2 standard product. *Atmospheric Measurement Techniques*, *10*(9), 3133.

Levelt, P. F., Joiner, J., Tamminen, J., Veefkind, J. P., Bhartia, P. K., Stein Zweers, D. C., Duncan, B. N., Streets, D. G., Eskes, H., van der A, R., McLinden, C., Fioletov, V., Carn, S., de Laat, J., DeLand, M., Marchenko, S., McPeters, R., Ziemke, J., Fu, D., Liu, X., Pickering, K., Apituley, A., González Abad, G., Arola, A., Boersma, F., Chan Miller, C., Chance, K., de Graaf, M., Hakkarainen, J., Hassinen, S., Ialongo, I., Kleipool, Q., Krotkov, N., Li, C., Lamsal, L., Newman, P., Nowlan, C., Suleiman, R., Tilstra, L. G., Torres, O., Wang, H. and Wargan, K. (2018). The Ozone Monitoring Instrument: overview of 14 years in space, Atmos. Chem. Phys., 18(8), 5699–5745, doi:10.5194/acp-18-5699-2018.

Levelt, P. F., van den Oord, G. H., Dobber, M. R., Malkki, A., Visser, H., de Vries, J., Stammes, P., Lundell, J.O.V., & Saari, H. (2006). The ozone monitoring instrument. IEEE Transactions on geoscience and remote sensing, 44(5), 1093-1101.

Li, C., Hsu, N. C., Sayer, A. M., Krotkov, N. A., Fu, J. S., Lamsal, L. N., ... & Tsay, S. C. (2016). Satellite observation of pollutant emissions from gas flaring activities near the Arctic. Atmospheric Environment, 133, 1-11.

Lin, J. T., McElroy, M. B., & Boersma, K. F. (2010). Constraint of anthropogenic NO x emissions in China from different sectors: a new methodology using multiple satellite retrievals. Atmospheric Chemistry and Physics, 10(1), 63-78.

Majid, A., Martin, M. V., Lamsal, L. N., & Duncan, B. N. (2017). A decade of changes in nitrogen oxides over regions of oil and natural gas activity in the United States. Elem Sci Anth, 5.

McDonald, B. C., Dallmann, T. R., Martin, E. W., & Harley, R. A. (2012). Long-term trends in nitrogen oxide emissions from motor vehicles at national, state, and air basin scales. *Journal of Geophysical Research: Atmospheres*, *117*(D21).

McDuffie, E. E., Edwards, P. M., Gilman, J. B., Lerner, B. M., Dubé, W. P., Trainer, M., Wolfe, D. E., Angevine, W. M., de Gouw, J. A., Williams, E. J., Tevlin, A. G., Murphy, J. G., Fischer, E. V., McKeen, S. A., Ryerson, T. B., Peischl, J., Holloway, J. S., Aikin, K. C., Langford, A. O., Senff, C. J., Alvarez, R. J., II, Hall, S. R., Ullmann, K., Lantz, K. O. and Brown, S. S. (2016). Influence of oil and gas emissions on summertime ozone in the Colorado Northern Front Range, J. Geophys. Res.-Atmos., 121, 8712–8729, doi:10.1002/2016JD025265.

Peischl, J., Eilerman, S., Neuman, J. A., Aikin, K. C., de Gouw, J. A., Gilman, J. B., Herndon, S. C., Nadkarni, R., Trainer, M., Warneke, C. and Ryerson, T. B. (2018). Quantifying methane and ethane emissions to the atmosphere from central and western U.S. oil and natural gas production regions, J. Geophys. Res.-Atmos., Submitted.

Russell, A. R., Valin, L. C., & Cohen, R. C. (2012). Trends in OMI NO 2 observations over the United States: effects of emission control technology and the economic recession. *Atmospheric Chemistry and Physics*, *12*(24), 12197-12209.

Schenkeveld, V. E., Jaross, G., Marchenko, S., Haffner, D., Kleipool, Q. L., Rozemeijer, N. C., ... & Levelt, P. F. (2017). In-flight performance of the Ozone Monitoring Instrument. *Atmospheric Measurement Techniques*, *10*(5), 1957.

Schnell, R. C., Oltmans, S. J., Neely, R. R., Endres, M. S., Molenar, J. V. and White, A. B. (2009). Rapid photochemical production of ozone at high concentrations in a rural site during winter, Nature Geosci., 2, 120–122.

Silva, R. A., West, J. J., Zhang, Y., Anenberg, S. C., Lamarque, J. F., Shindell, D. T., ... & Horowitz, L. W. (2013). Global premature mortality due to anthropogenic outdoor air pollution and the contribution of past climate change. Environmental Research Letters, 8(3), 034005.

USEIA (2018a), U.S. Energy Information Administration, 4 April. [Available at https://www.eia.gov/dnav/pet/hist/LeafHandler.ashx?n=PET&s=MCRFPUS1&f=M]

USEIA (2018b), U.S. Energy Information Administration, 4 April. [Available at https://www.eia.gov/dnav/ng/hist/n9050us2m.htm]

USEIA (2018c), U.S. Energy Information Administration, Annual energy outlook 2018, 6 February. [Available at https://www.eia.gov/outlooks/aeo/pdf/AEO2018.pdf]

USEIA (2018d), U.S. Energy Information Administration, "Independent Statistics & Analysis, Drilling Productivity Report", 4 April. [Available at http://www.eia.gov/petroleum/drilling/pdf/dpr-full.pdf]

Van der A, R. J., Eskes, H. J., Boersma, K. F., Van Noije, T. P. C., Van Roozendael, M., De Smedt, I., ... & Meijer, E. W. (2008). Trends, seasonal variability and dominant NOx source derived from a ten-year record of NO2 measured from space. Journal of Geophysical Research: Atmospheres, 113(D4).

Warneke, C., Trainer, M., de Gouw, J. A., Parrish, D. D., Fahey, D. W., Ravishankara, A. R., ... & Neuman, J. A. (2016). Instrumentation and measurement strategy for the NOAA SENEX aircraft campaign as part of the Southeast Atmosphere Study 2013.

WHO (2005). World Health Organization, Air quality guidelines, global update 2005: particulate matter, ozone, nitrogen dioxide and sulfur dioxide.

Supplemental Information
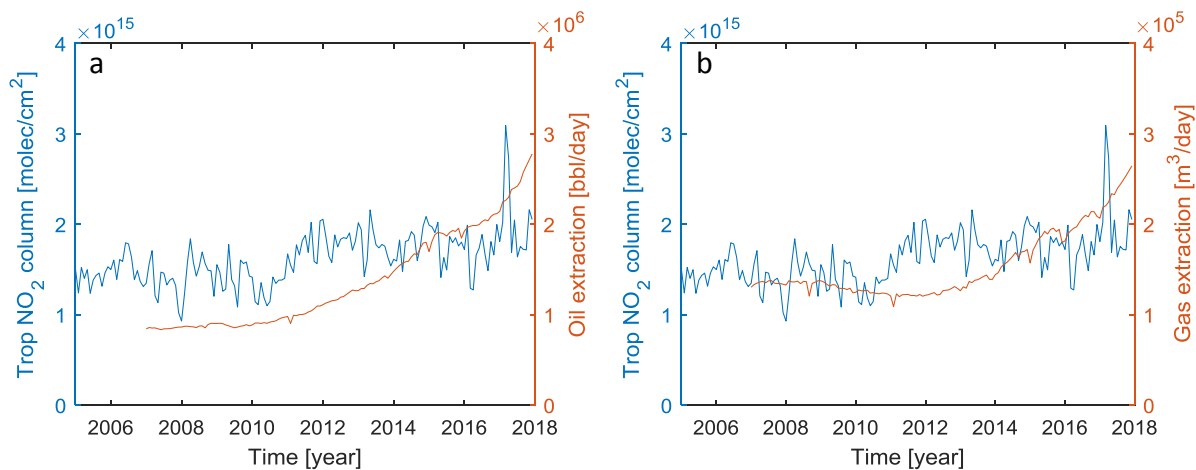
Figure S9 The tropospheric NO$_2$ column time series (x10^{15} molecules/cm^2) in the Permian, averaged per month, from 2005 to 2018 (blue) plotted with (A) the extraction of oil and (B) the extraction of gas from 2007 to 2018 (orange). The seasonal variation is removed from the NO$_2$ time series.
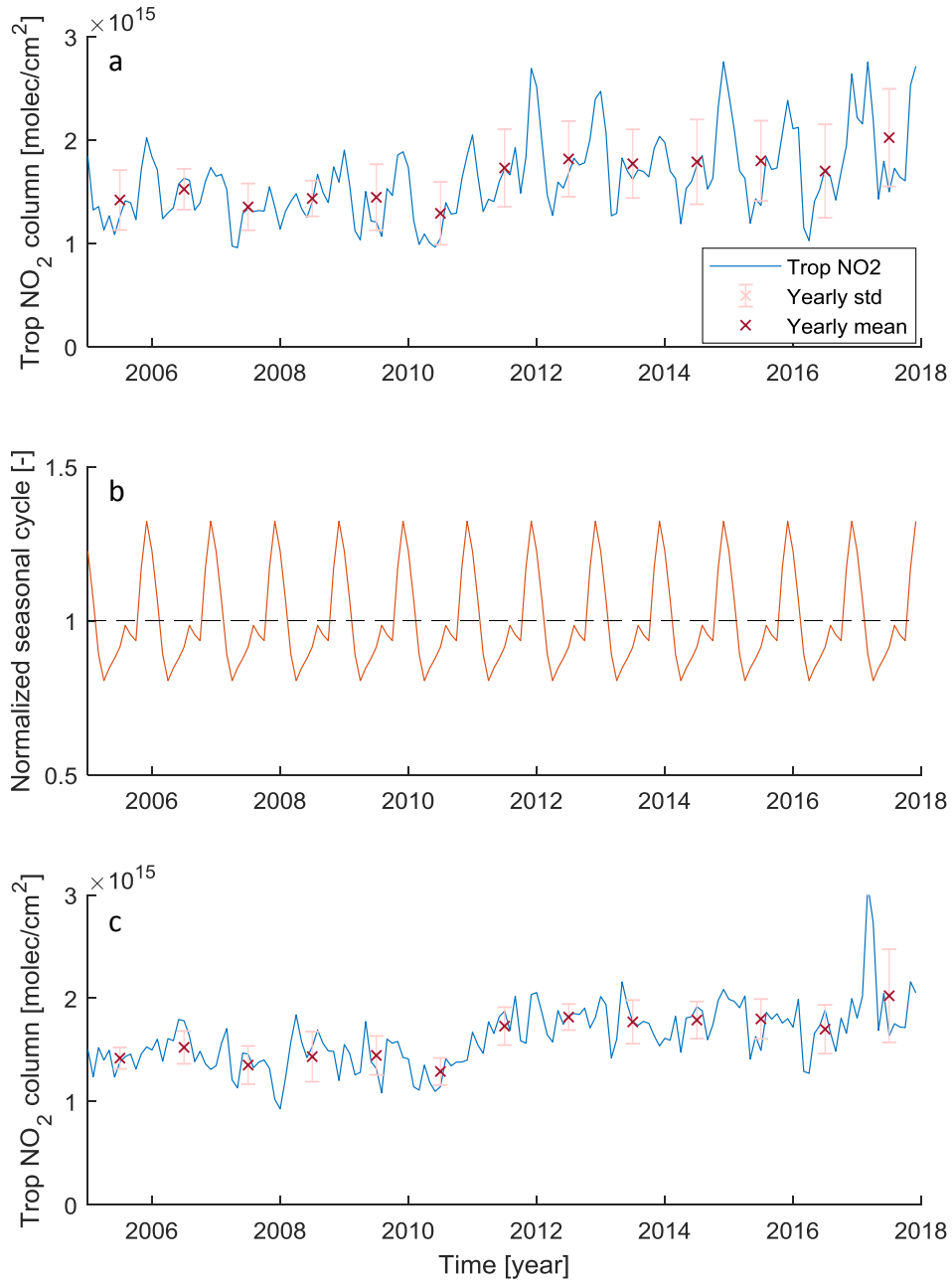
Figure S10 The tropospheric NO$_2$ column time series in the Permian region before removal of the seasonal variation (a) and after the removal of the seasonal variation (c). The normalized seasonal cycle (b) removes the seasonal trend from the time series by division. The red crosses and error bars represent the yearly averages and standard deviations of the measured NO$_2$ time series.
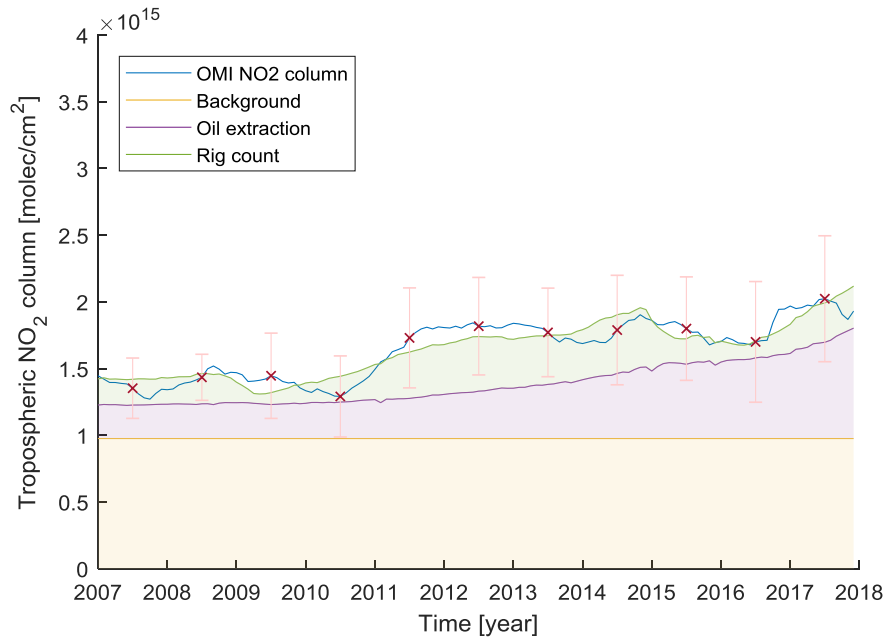
Figure S11 The tropospheric NO$_2$ column time series in the Permian region after removing the seasonal trend using a 12-month moving average (r^2=0.84) (blue) and the modelled NO$_2$ time series separated in a constant background column (yellow), an NO$_2$ column caused by extraction of oil (purple) and an NO$_2$ column caused by drilling (green) in the Bakken region. The red crosses and error bars represent the yearly averages and standard deviations of the measured NO$_2$ time series. The black dot represents the SONGNEX column described in Section 3.3.
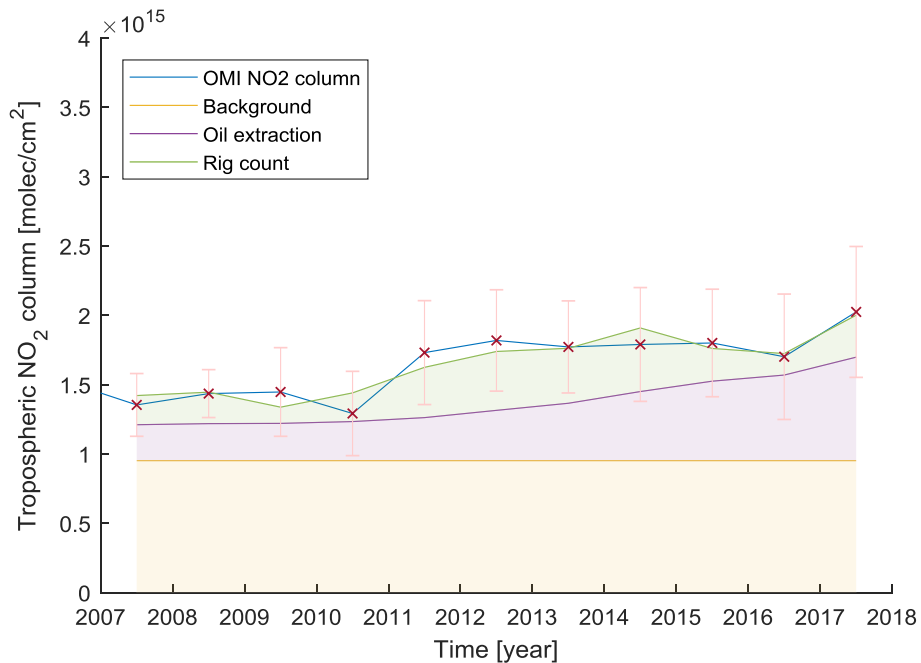
Figure S12 The tropospheric NO$_2$ column time series in the Permian region using yearly averaged data where no removal of the seasonal variation is necessary (r^2=0.86) (blue) and the modelled NO$_2$ time series separated in a constant background column (yellow), an NO$_2$ column caused by extraction of oil (purple) and an NO$_2$ column caused by drilling (green) in the Bakken region. The red crosses and error bars represent the yearly averages and standard deviations of the measured NO$_2$ time series. The black dot represents the SONGNEX column described in Section 3.3.
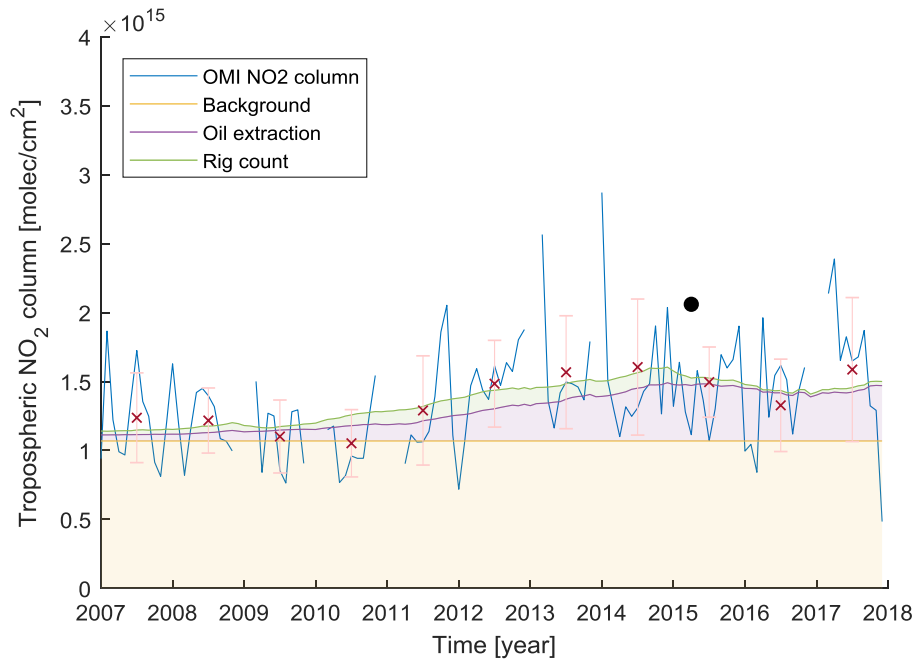
Figure S13 The measured tropospheric OMI NO_2 column time series (blue) and the modelled NO_2 time series separated in a constant background column (yellow), an NO_2 column caused by extraction of oil (purple) and an NO_2 column caused by drilling (green) in the Bakken region. The red crosses and error bars represent the yearly averages and standard deviations of the measured NO_2 time series. The black dot represents the SONGNEX column described in Section 3.3.
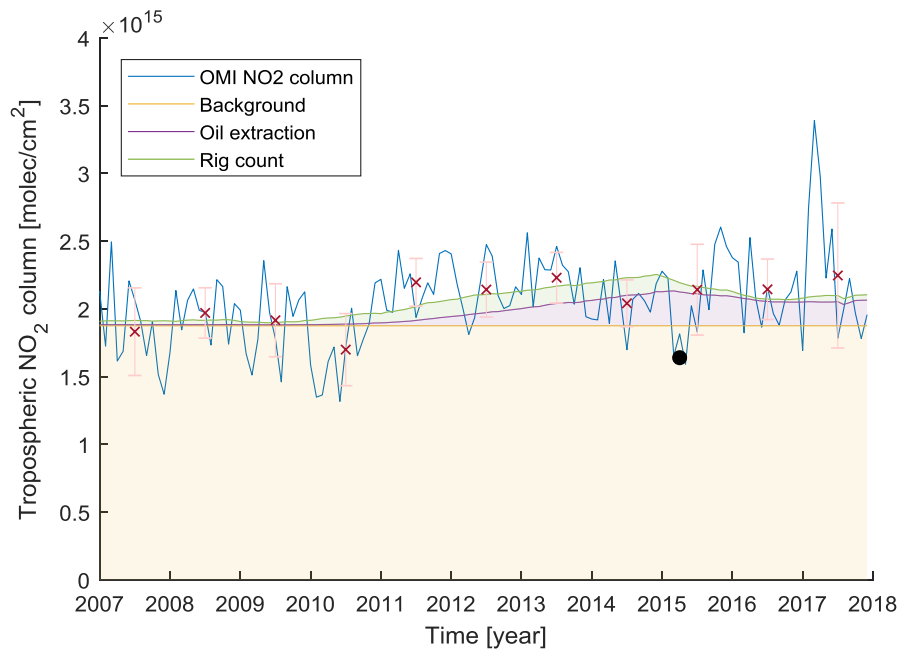
Figure S14 The measured tropospheric OMI NO_2 column time series (blue) and the modelled NO_2 time series separated in a constant background column (yellow), an NO_2 column caused by extraction of oil (purple) and an NO_2 column caused by drilling (green) in the Eagle Ford region. The red crosses and error bars represent the yearly averages and standard deviations of the measured NO_2 time series. The black dot represents the SONGNEX column described in Section 3.3.
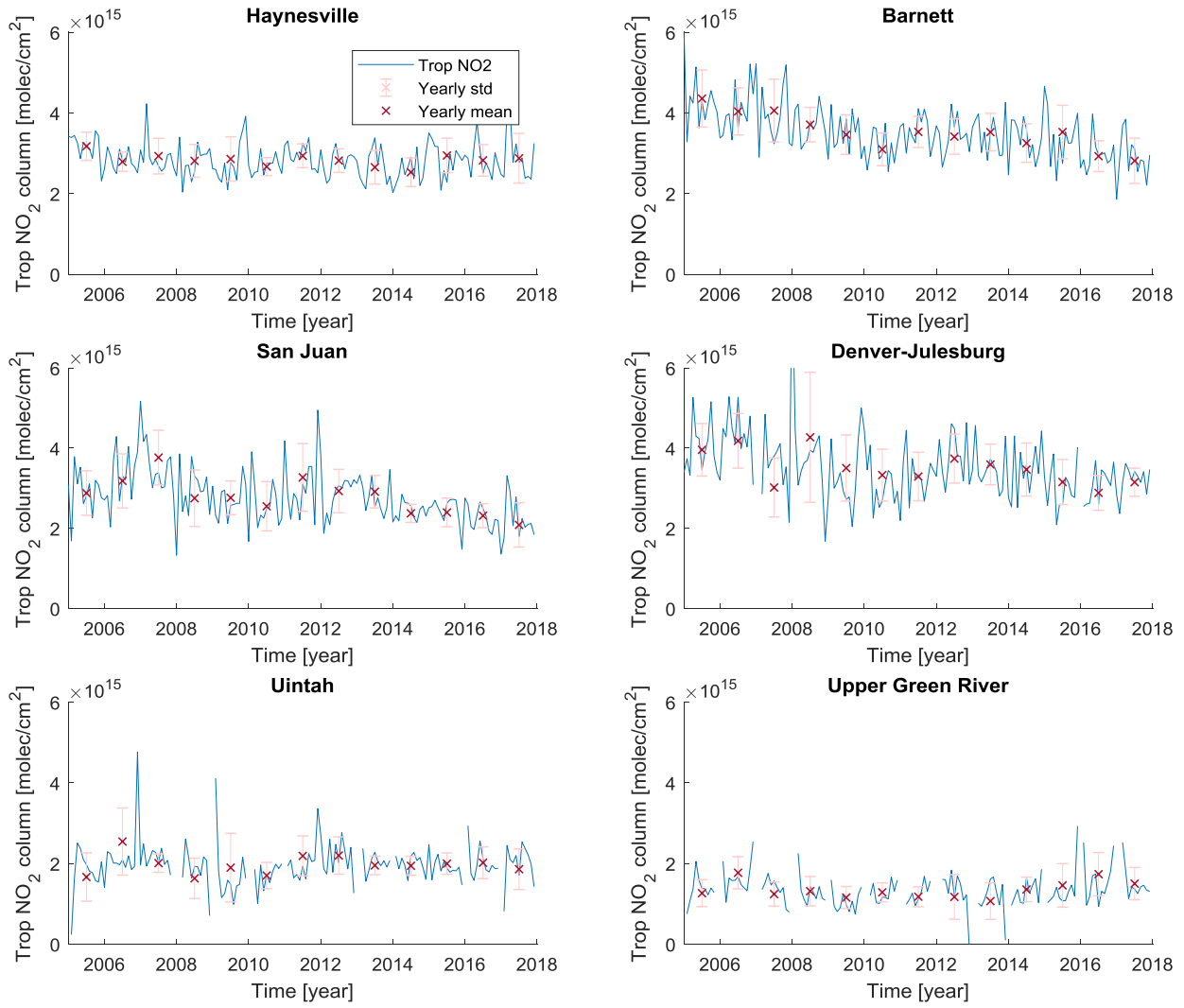
Figure S15 The tropospheric NO$_2$ column time series after removal of the seasonal variations for the Haynesville, Barnett, San Juan, Denver-Julesburg, Uintah and Upper Green River extraction regions. The red crosses and error bars represent the yearly averages and standard deviations of the measured NO$_2$ time series.
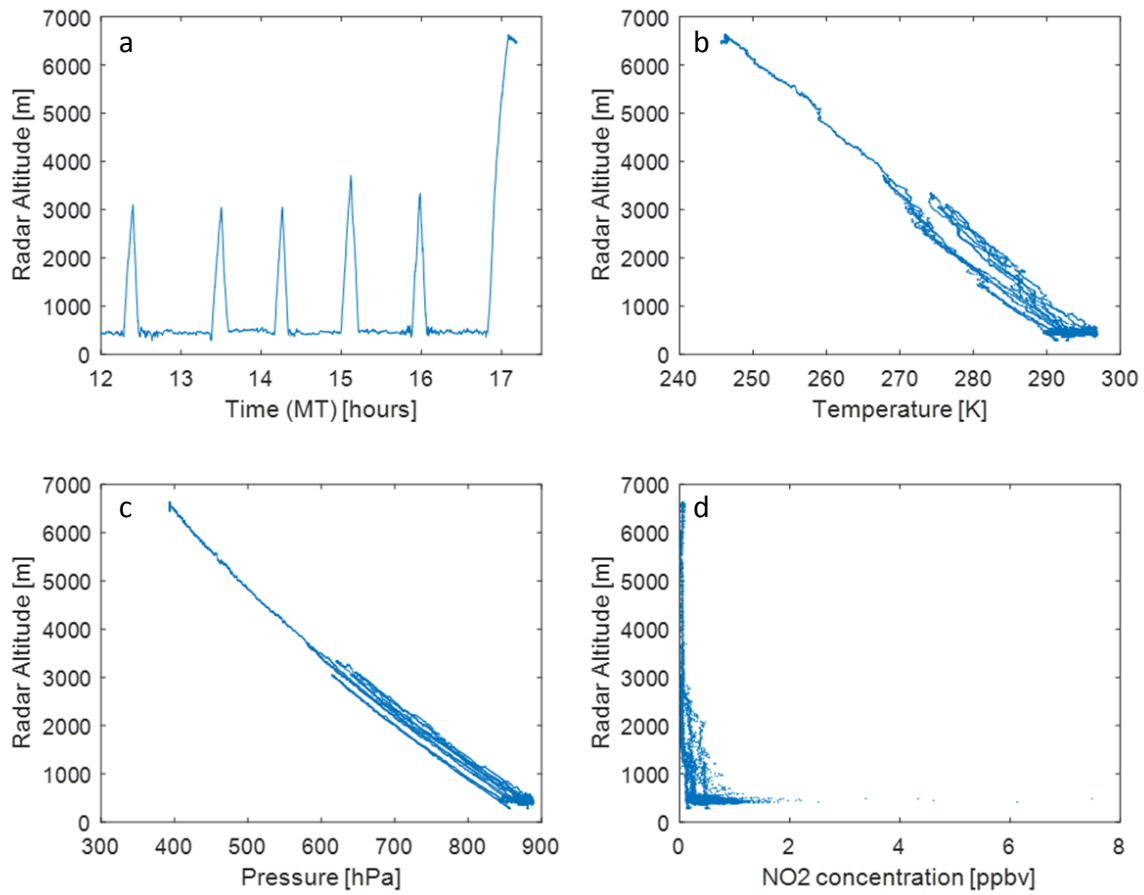
Figure S16 The SONGNEX results in the Permian region showing the altitude as function of time (a), of temperature (b), of pressure (c) and of the measured NO_2 concentration in parts per billion volume (d). In (a) you can see the peaks the aircraft made in order to get a good vertical measurement distribution. The last peak is highest and happens before the aircraft takes off to fly back to the airport. The temperature and pressure are necessary to convert the NO_2 concentration from ppbv to molecules/cm^3 using the ideal gas law. After the conversion, the measurements are averaged over height using a bin size of 500 m to get an NO_2 profile as shown in Figure 8.
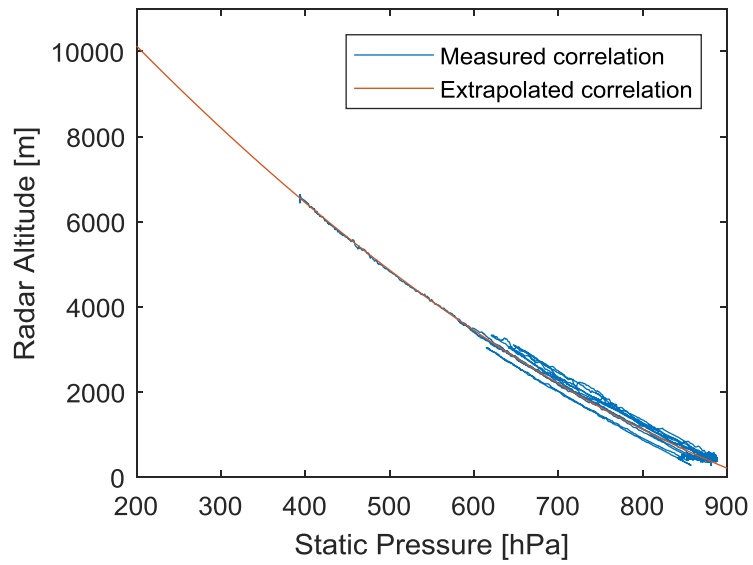
Figure S17 The altitude as function of pressure extrapolated till a pressure level of 200 hPa. This point corresponds with an altitude of 10 km which is assumed the altitude of the tropopause.